



## ORIGINAL ARTICLE

# Assessing the bearing capacity of Crestbond shear connectors to concrete pry-out

## *Resistência à ruptura do concreto por pry-out em conectores de cisalhamento Crestbond*

Ricardo Laguardia Justen de Almeida<sup>a</sup> Gustavo de Souza Veríssimo<sup>a</sup> José Carlos Lopes Ribeiro<sup>a</sup> José Luiz Rangel Paes<sup>a</sup> Rodrigo Barreto Caldas<sup>b</sup> Hermano de Sousa Cardoso<sup>c</sup> Ricardo Hallal Fakury<sup>b</sup> <sup>a</sup>Universidade Federal de Viçosa – UFV, Departamento de Engenharia Civil, Viçosa, MG, Brasil<sup>b</sup>Universidade Federal de Minas Gerais – UFMG, Programa de Pós-graduação em Engenharia de Estruturas, Belo Horizonte, MG, Brasil<sup>c</sup>Universidade de Coimbra, Institute for Sustainability and Innovation in Structural Engineering – ISISE, Department of Civil Engineering, Coimbra, Portugal

Received 04 November, 2021

Accepted 09 May 2022

**Abstract:** In this work, a study on failure by concrete pry-out in Crestbond shear connectors is presented. The study's aim was the development of an expression that estimates the connection's bearing capacity. The analyses were carried out through numerical simulations designed to reproduce the referred failure mode. Numerical and experimental results are compared and discussed in relation to the maximum force reached and the cracking aspect typical of concrete pry-out. The proposed equation corresponded well to experimental results, with a mean ratio  $P_{theo}/P_{exp}$  equal to 0,99 and a coefficient of variation of 10%. The results found in this study indicate that the concrete pry-out expression in German Technical Approval Z-26.4-56 can also be applied to Crestbond shear connectors.

**Keywords:** shear connector, Crestbond, numerical model, concrete pry-out, composite dowels.

**Resumo:** Neste trabalho é apresentado um estudo sobre a ruptura do concreto por pry-out em conectores de cisalhamento tipo Crestbond com o objetivo de obter um modelo de cálculo que estima a resistência da conexão a esse modo de falha. As análises foram realizadas por meio de simulações numéricas capazes de reproduzir o referido modo de falha. Os resultados numéricos são comparados com os experimentais e discutidos em relação à força máxima atingida e o aspecto da fissuração típica do pry-out. O modelo de cálculo proposto apresentou boa correspondência com os resultados experimentais, com uma razão média  $P_{teo}/P_{exp}$  igual a 0,99 e um coeficiente de variação de 10%. Os valores encontrados nesse estudo sugerem que a expressão da Aprovação Técnica Alemã para outros conectores pode ser aplicada nos conectores Crestbond.

**Palavras-chave:** conector de cisalhamento, Crestbond, modelo numérico, pry-out do concreto, composite dowels.

**How to cite:** R. L. J. Almeida et al., "Assessing the bearing capacity of Crestbond shear connectors to concrete pry-out," *Rev. IBRACON Estrut. Mater.*, vol. 16, no. 1, e16107, 2023, <https://doi.org/10.1590/S1983-41952023000100007>

**Corresponding author:** Ricardo Laguardia Justen de Almeida. E-mail: ricardoljalmeida@gmail.com

**Financial support:** Coordenação de Aperfeiçoamento de Pessoal de Nível Superior (CAPES) – Finance Code 001; Universidade Federal de Viçosa.

**Conflict of interest:** Nothing to declare.

**Data Availability:** The data that support the findings of this study are available from the corresponding author, R. A., upon reasonable request.



This is an Open Access article distributed under the terms of the [Creative Commons Attribution License](https://creativecommons.org/licenses/by/4.0/), which permits unrestricted use, distribution, and reproduction in any medium, provided the original work is properly cited.

## 1 INTRODUCTION

In recent years there has been a lot of research, especially as part of a European project called PreCo-Beam, to investigate the structural behavior of composite dowels [1]-[8], among which two shear connectors stand out due to their structural performance: the puzzle connector (PZ) - Figure 1b - and the clothoidal connector (MCL) - Figure 1c. In Brazil, a third shear connector was studied by Verissimo [9], called Crestbond (CR) - Figure 1a.

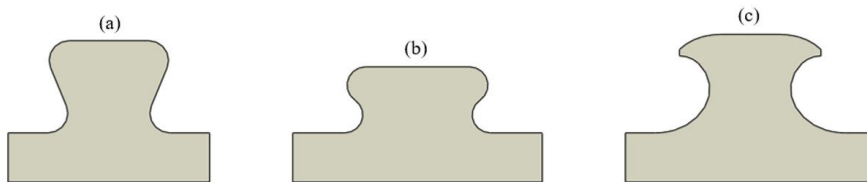


**Figure 1.** Composite dowel shear connection geometries: (a) Crestbond (CR); (b) Puzzle (PZ) and (c) Clothoidal (MCL).

Crestbond was developed due to the difficulties associated with the installation of the usual connectors in Brazil (shear-stud and C-channel) and has been the subject of research over the last few years [10]-[16]. Crestbond's geometry is similar to that of connectors studied in the PreCo-Beam project [5], particularly the puzzle shear connector. However, the Crestbond shear connector may have a different structural behavior due to its greater slenderness.

Because of the complex geometry of shear connectors, the heterogeneous behavior of concrete, and the interaction between these two elements, the strength mechanism of composite dowels cannot be sufficiently described through experimental tests alone. Therefore, a significant part of this research was carried out through numerical models capable of simulating the nonlinearities of the materials and contact interactions to better understand the behavior of composite dowels [7], [17]-[20].

The bearing capacity of composite dowels is limited to three failure modes [21]: (a) concrete shearing, (b) concrete pry-out, and (c) steel failure. Currently, German Technical Approval Z-26.4-56 [22] establishes design equations concerning these failure modes for the PZ and MCL geometries. On the other hand, the only expressions available for Crestbond failure modes are those pertaining to concrete shearing and steel failure [9], [14], [16], [23]. This work aims to suggest an expression to estimate Crestbond's bearing capacity to concrete pry-out, a third failure mode, through finite element modelling (FEM). To achieve this objective, the research was divided in two parts: (i) development and validation of a numerical model representing push-out tests with Crestbond shear connectors and (ii) a parametric study of factors that directly affect concrete pry-out resistance. Combined with the already established equations for concrete shearing and steel failure in Crestbond, a new expression that solves the matter of concrete pry-out would allow for the design and application of Crestbond shear connectors in steel-concrete composite structures.

## 2 CONCRETE PRY-OUT FAILURE MODE

Concrete pry-out occurs when the shear connector is not deeply embedded in the slab, *i.e.*, when concrete cover over the connector is small (parameters  $c_t$  or  $c_b$  of Figure 2). Once under load, the concrete confined in the connector's openings becomes more resistant to compression than the concrete above the connector. This results in forces aimed towards the smallest height of concrete ( $h_{po}$ ). When the shear stresses exceed the shear strength of the concrete, a cone-shaped portion of concrete detaches from the slab (Figure 3) leading to the connection's failure [21], [24].

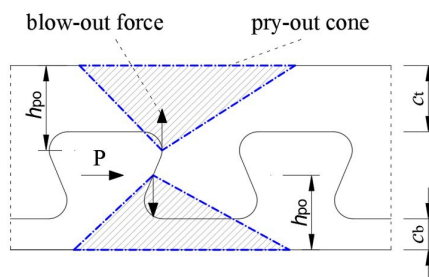


**Figure 2.** Idealization of concrete pry-out in Crestbond shear connectors.

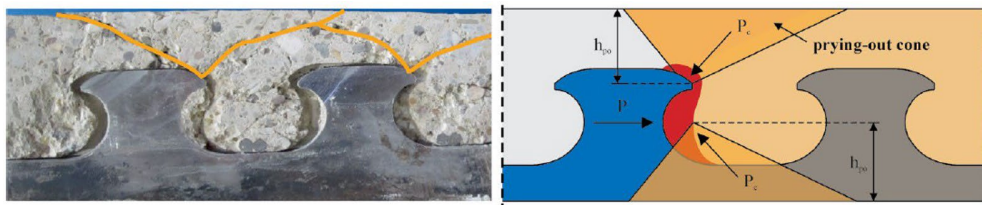


Figure 3. Concrete pry-out failure in MCL shear connectors – Feldmann et al. [2].

Since this failure mode was discovered, design equations have been proposed to estimate the connection’s resistance to concrete pry-out [25]-[27]. These equations were established in German Technical Approval Z-26.4-56 [22], which contains all usage guidelines for MCL and PZ shear connectors. The design equation for concrete pry-out is presented in Equation 1:

$$P_{po,k} = 90(1 + \rho_{D,i}) \chi_x \chi_y \sqrt{f_{ck}} h_{po}^{1.5} \tag{1}$$

where:  $f_{ck}$  – compressive strength of the concrete [MPa];  $h_{po}$  – height of the pry-out cone [mm];  $P_{po,k}$  – characteristic resistance to concrete pry-out [N/dowel].

The reduction factors  $\chi_x$  and  $\chi_y$  consider the overlapping of the concrete cones in the longitudinal and transverse directions, respectively, and are determined according to Equation 2. In the case of a single row of connectors, factor  $\chi_y$  is equal to 1,0.

$$\chi_x = \frac{e_x}{4,5 h_{po}} \leq 1 \quad \chi_y = \frac{1}{2} \left( \frac{e_y}{9 h_{po}} + 1 \right) \leq 1 \tag{2}$$

The term  $\rho_{D,i}$  (Equation 3) considers the influence of the effective reinforcement ratio ( $A_b + A_t = A_{ef}$ ), i. e., reinforcement passing through the opening and above the shear connector (Figure 4):

$$\rho_{D,i} = \frac{E_s A_{ef}}{E_{cm} A_{D,i}} \tag{3}$$

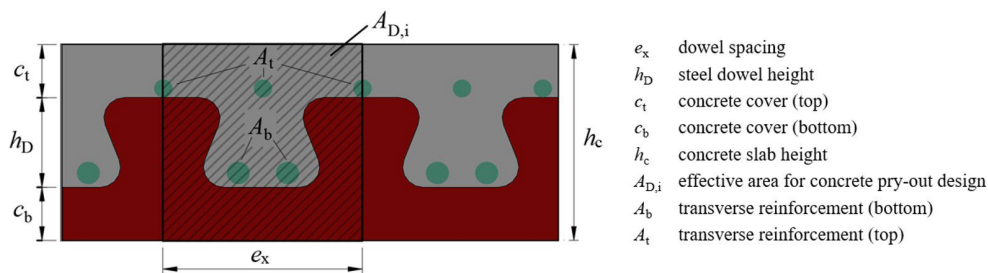


Figure 4. Parameters of composite dowels.

According to Z-26.4-56 [22], the height of the concrete cone ( $h_{po}$ ) for both MCL and PZ geometries is determined as follows (Equation 4):

$$h_{po} = \min(c_t + 0,07 e_x; c_b + 0,13 e_x) \tag{4}$$

It should be mentioned, however, that Equation 1 estimates the characteristic resistance of composite dowels to concrete pry-out, and a large set of experimental results is required to develop expressions at characteristic-level. These expressions can be obtained through the method presented in Annex D of EN 1990:2002 [28], which converts the

engineering model (the mean value) to design load level. In this research, the expression at the mean-level was used as presented at Equation 5 [21]:

$$P_{po} = k \frac{1}{\eta} (1 + \rho_{D,i}) \chi_x \chi_y \sqrt{f_{ck}} h_{po}^{1,5} \tag{5}$$

The factor  $1/\eta$  was initially proposed by Heinemeyer [27] and depends significantly on the concrete strength (Equation 6). In German Technical Approval Z-26.4-56 [22], this factor was replaced by a constant value determined for the lowest concrete class (C20/25).

$$\eta = 0,4 - 0,001f_c \tag{6}$$

The coefficient ‘ $k$ ’ in Equation 5 takes into consideration assumptions made for the construction of the expression, such as the admission of  $\sqrt{f_{ck}}$  as the concrete’s tensile strength and of parameter  $h_{po}^{1,5}$ , which estimates the surface area of the pry-out cone [24]. This coefficient, defined through a regression analysis, significantly affects the quality of the mechanical model, which is why an extensive database is needed for its determination. According to Kopp et al. [21], a value of 40,44 was obtained through experiments for puzzle and clothoidal shear connectors.

### 3 EXPERIMENTAL PROGRAM

The experimental program conducted in the developmental stages of the Crestbond shear connector involved 41 push-out tests, which were divided into four series (A, B, C, and D) and performed according to the specifications of EN-1994-1-1:2004 [29].

The purpose of the experimental program’s series A was to evaluate the connector’s behavior from a qualitative standpoint in order to define the parameters that would be employed in subsequent tests. With the results obtained in this series, Verissimo [9] developed the CR56b shear connector used in series B and C. These series were performed in order to understand the behavior of the CR56b connector, including its shear capacity, failure modes, and ductility. Series C is identical to series B, except for the concrete’s strength. The third stage of the experimental program (series D), object of study of this work, was handled by Oliveira [30] and includes tests that simulate the presence of a pre-slab, given the widespread use of composite floor systems with prefabricated concrete slabs in Brazil. In series D, specimens were assembled with a real concrete pre-slab (Figure 5a); with EPS (expanded polystyrene) plates in place of the pre-slab (Figure 5b); and without a pre-slab (Figure 5c). Fifteen tests were performed, divided into five groups, identified in Table 1. Dimensions of the shear connector used in series D (CR56b-PL) and the setup of the experiments are shown in Figure 6. The shear connectors were 12mm thick in all series.

**Table 1.** Parameters and description of specimens.

Group	Nomenclature	Description	Specimen	$f_{cm}$ [MPa]	$A_b$	$A_t$	$c_b$ [mm]	$c_t$ [mm]
D1	CR56b-PL30EPS-As0	30 mm thick EPS plate and no reinforcement	D1.a/D1.b/D1.c	31,6/31,3/31,3	-	-	30	33,8
D2	CR56b-PL30EPS-As8	30 mm thick EPS plate with reinforcement	D2.a/D2.b/D2.c	31,4/31,4/31,3	1 $\phi$ 8,0	1 $\phi$ 8,0	30	33,8
D3	CR56b-PL30-As0	30 mm thick concrete pre-slab and no reinforcement	D3.a/D3.b/D3.c	31,6/32,4/31,1	-	-	-	33,8
D4	CR56b-PL45EPS-As0	45 mm thick EPS plate and no reinforcement	D4.a/D4.b/D4.c	32,6/32,2/32,2	-	-	15	33,8
D5	CR56b-As0	no pre-slab and no reinforcement	D5.a/D5.b/D5.c	22,2/32,1/31,3	-	-	-	33,8



Figure 5. Specimens tested: (a) concrete pre-slab; (b) EPS plate and (c) no pre-slab.

All specimens had longitudinal reinforcement and additional transverse reinforcement arranged close to the regions of support and load application. No reinforcement was placed inside the openings of the shear connector, except for group D2.

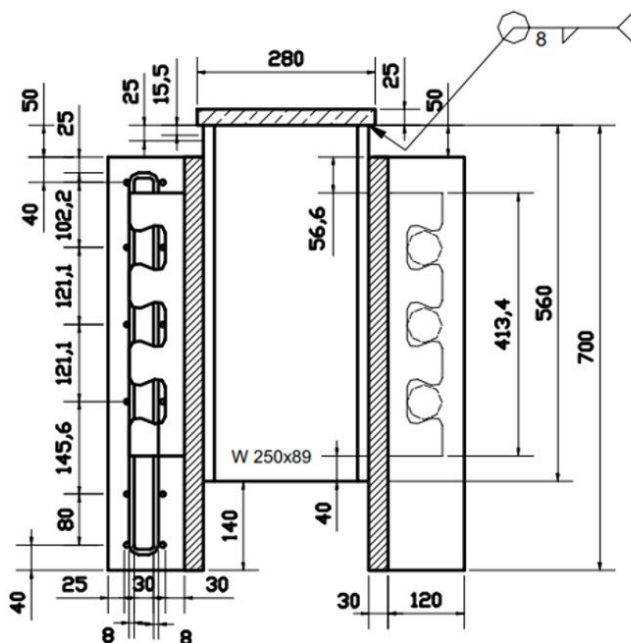


Figure 6. Dimensions of specimens (in mm) and experiment setup (group D2).

## 4 NUMERICAL ANALYSES

Numerical simulations were performed using finite element package ABAQUS, used by several authors to study the behavior of shear connectors [14], [17], [19], [20], [31], [32]. The description of the numerical model is presented in the subsequent sections.

### 4.1 Development and validation of the numerical model

#### 4.1.1 Geometry and boundary conditions

Due to its double symmetry, only a quarter of the specimen was modeled to reduce computational effort. The base of the slab was fixed to prevent displacement in the normal direction ( $U_z = 0$ ) and symmetry conditions were applied to the symmetry planes (Figure 7). The analysis was performed by means of displacement control, which was applied to the steel profile's cross section.

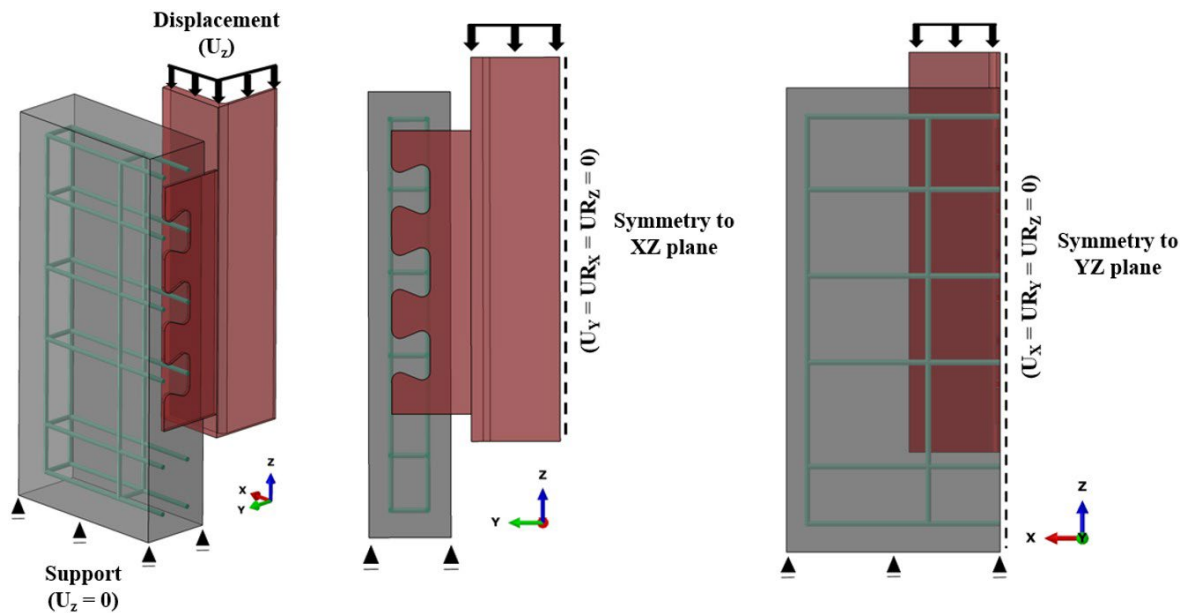


Figure 7. Geometry and boundary conditions of the numerical model (group D2).

Contact between the concrete slab and the steel components was simulated through the “hard contact” interaction in the normal direction. In the tangential direction, an interaction that admits friction (penalty) between the elements was adopted, with a friction coefficient of  $\mu = 0,3$  (Figure 8). Values between 0,3 and 0,5 are recommended for this type of analysis by Fink et al. [33] who investigated the value of this coefficient through an extensive parametric study. Other authors also adopt the value of 0,3 in numerical simulations of continuous shear connectors with regular openings [8], [20].

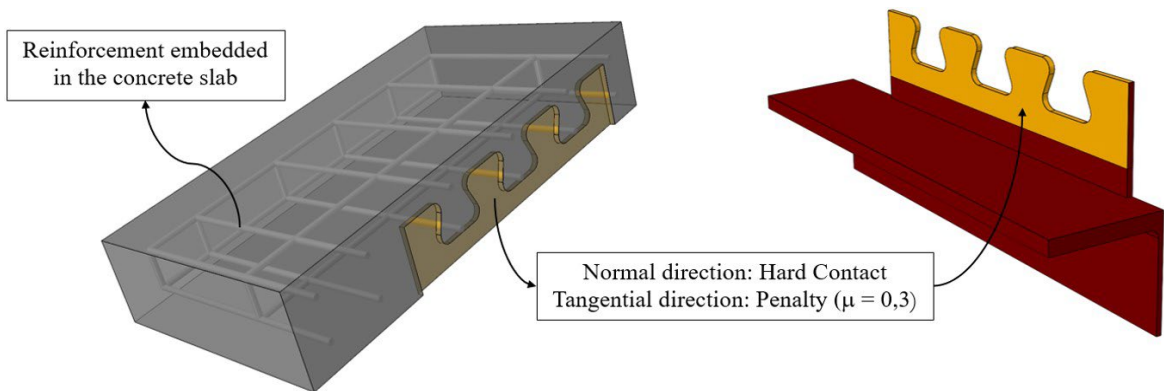
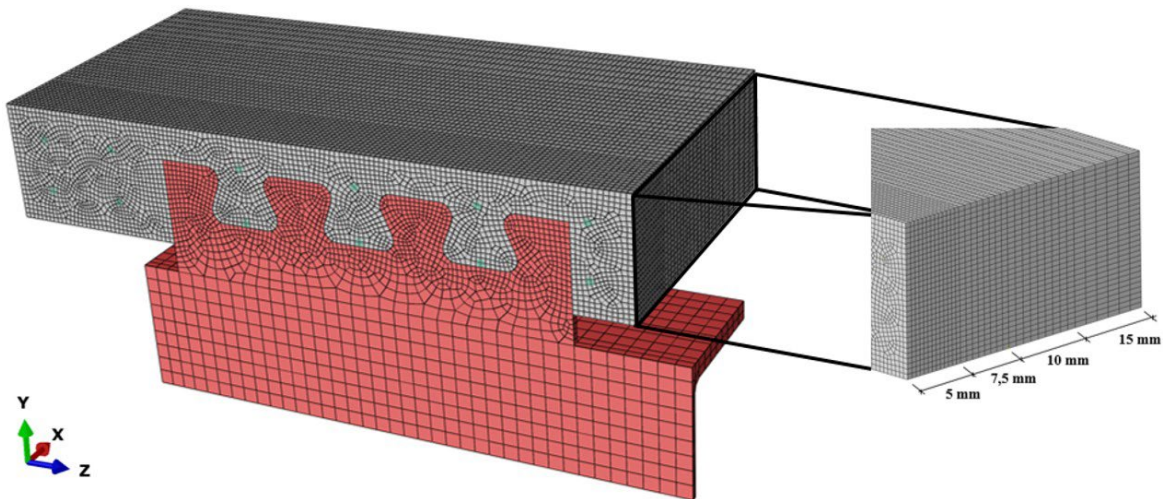


Figure 8. Interactions in the numerical model (Group D2).

In the specimens of groups D3 and D5, which include, respectively, a concrete pre-slab and no pre-slab, the interaction extends until the upper flange of the steel profile. The contact between the elements was simulated using the penalty contact formulation, and the perpendicular forces of contact between the shear connector and the concrete slab were determined through the finite sliding formulation, which investigates possible contact pairs between the nodes of the elements throughout the analysis [7]. The reinforcement was configured completely embedded in the concrete slab, so that the translational degrees of freedom of the reinforcement were coupled to the nodes of the surrounding concrete.

#### 4.1.2 Finite elements mesh

A mesh convergence study was conducted to determine the finite elements' size, which also took into consideration the meshes used by Dutra [23] and Silva [34] in their numerical modeling of the Crestbond shear connector. In the transverse direction of the concrete slab, element sizes began at 5 mm around the connection and increased up to 15 mm towards the edge of the slab (Figure 9). In the longitudinal direction, the size was fixed at 5 mm. The steel profile and the shear connector were discretized into 15 and 5 mm elements, respectively. These components were modeled with solid C3D8R elements, with eight nodes and reduced integration, as the C3D8R is more appropriate for performing explicit dynamic analyses [34]. The slab reinforcement was modeled as a B31 beam element, with two nodes, and discretized into 10 mm elements.



**Figure 9.** Finite element mesh.

#### 4.1.3 Analysis method

Numerical simulations were performed through explicit dynamic analysis, recommended for very non-linear problems, where large deformations and contact interactions occur, which is the case in push-out tests [20]. Unlike implicit numerical methods (such as the usual Newton-Raphson), the explicit analysis is based on dynamic equilibrium, being frequently employed in problems involving concrete cracking and steel lamination. In the explicit dynamic analysis method, the global mass and stiffness matrices do not need to be allocated and inverted, which means that each increment results in less computational effort in comparison to the implicit analysis [23]. The most important aspect of any explicit dynamic analysis is the size of the smallest finite element in the model, since it represents an estimate of the time increment size once divided by the material's wave propagation velocity [35]. This type of analysis is generally used to model events called “quasi-static”, in which the loading rate is small enough so that the inertial forces are negligible. However, a quasi-static analysis can be extremely long when modeled in real-time, requiring large computational resources. Therefore, the analysis speed is artificially increased to obtain an economically viable solution. ABAQUS offers two methods for reducing analysis processing time: time scaling and mass scaling. These methods, however, tend to increase the inertial forces in the numerical model, which can lead to unrealistic results. In this research, mass scaling was employed with a desired time increment of 0,005s, determined through preliminary analyses in order to provide the shortest possible analysis time with insignificant inertial forces [35]. This method artificially increases the mass of the elements so that the time increments are less than or equal to the time increment technically necessary for a quasi-static condition.

A quasi-static solution can also be attained through gradually applied loads or displacements. The application of an external action can induce the propagation of stress waves throughout the model, compromising the simulation's accuracy [35]. Thus, a displacement was applied based on a smooth curve in order to decrease inertial forces. ABAQUS creates a fifth-order transition polynomial between two extreme values, so that the first and the second derivatives are zero at the beginning and end of the transition. The displacement-rate adopted was 0,02 mm/s, similar to the real displacement-rate used in the experiments.

One way to verify if the numerical simulation truly reflects a quasi-static analysis is to balance the numerical model’s energy. In general, the kinetic energy of the model should not exceed a small fraction (1-10%) of its internal energy throughout most of the analysis. In other words, the work exerted by external forces must be nearly equal to the internal energy of the system [35]. This balance is usually not present at the beginning of analyses, as parts of the model will be moving before any significant deformations develop.

#### 4.1.4 Materials

##### 4.1.4.1 Concrete

The non-linear behavior of concrete was simulated using the Concrete Damaged Plasticity (CDP) model implemented in the ABAQUS library. This model is widely used in numerical studies of shear connectors, and in this research its input parameters were adopted according to literature recommendations [8], [20], [32], [33], [36] as shown in Figure 10. The behavior of concrete under compression was simulated using the stress-strain relationship proposed by Pavlovic et al. [32], which adopts an extension of the curve presented in EN 1992 1 1:2010 [37], limited to an ultimate strain  $\epsilon_{cu1} = 3,5\%$ . This strain is not a problem in conventional reinforced concrete structures since, in general, deformations in these structures remain below this value. In push-out tests, on the other hand, the concrete inside the openings undergoes large deformations and resists high compressive three-dimensional stresses, which produce a confinement effect in this region. In this situation, the behavior of the concrete becomes highly dependent on the descending branch of its stress-strain relationship. An ultimate strain of  $\epsilon_{cu1} = 3,5\%$  would lead to unrealistic stresses in the concrete, overestimating the connector’s strength. The extension proposed by Pavlovic et al. [32] involves a series of parameters and is divided into two branches: sinusoidal and linear (Figure 10). The parameters were calibrated so that the numerical results would be as close as possible to the experimental ones.

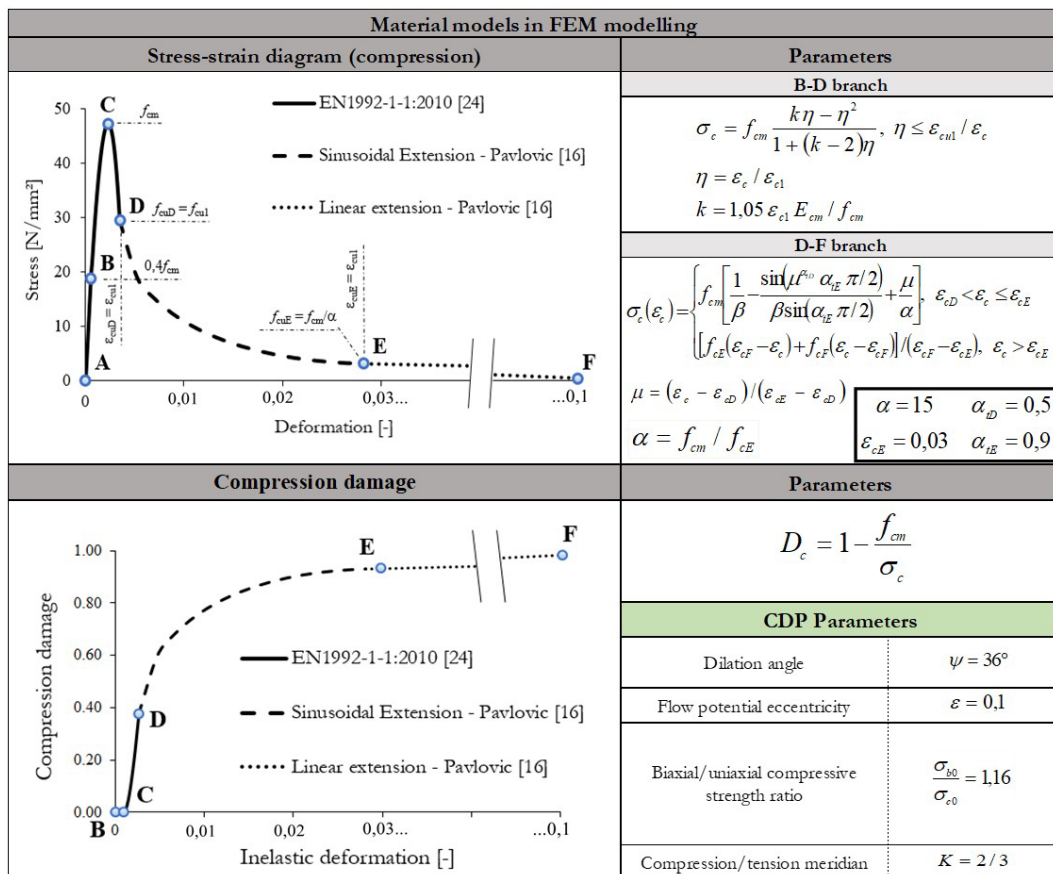


Figure 10. Material model for compression and CDP model parameters.

The numerical model was configured to take into consideration any damage suffered by the compressed concrete, which starts when the deformation in the concrete exceeds the deformation corresponding to the concrete strength ( $\epsilon_{c1}$ ).

The tensile behavior of concrete was represented by a stress-crack width model proposed by Hordijk [38]. In this model, the concrete response is governed by an exponential function (Figure 11).

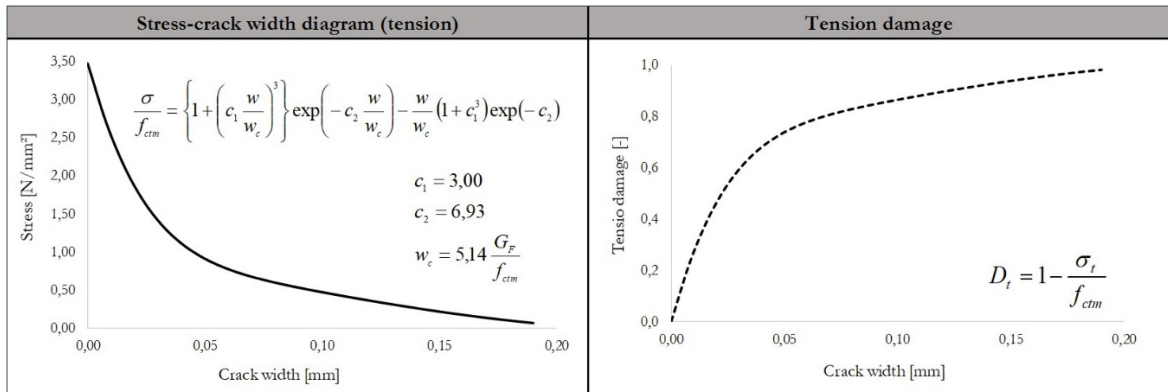


Figure 11. Material model for tension.

Fracture energy ( $G_f$ ) was determined according to Model Code 2010 [39], while other properties necessary for implementing the behavior of concrete in the numerical model (such as modulus of elasticity –  $E_{cm}$ ; mean tensile strength –  $f_{ctm}$ ; and strain associated with the maximum compressive stress –  $\epsilon_{c1}$ ) were determined according to the equations presented in EN 1992 1 1:2010 [37]. The compressive strength was adopted as the mean value between models of the same group (Table 1).

#### 4.1.4.2 Steel components

The properties of the steel components (shear connector, reinforcement, and steel profile) are shown in Figure 12. Elasto-plastic diagrams were used for the reinforcement (CA-50 steel) and steel profile materials (ASTM A572 Grade 50), while a hardening modulus ( $E_h$ ) equal to 2700 N/mm<sup>2</sup> was adopted for the shear connector. This artificial modelling was suggested by Byfield and Dhanalakshmi [40] for occasions where no material characterization tests are available.

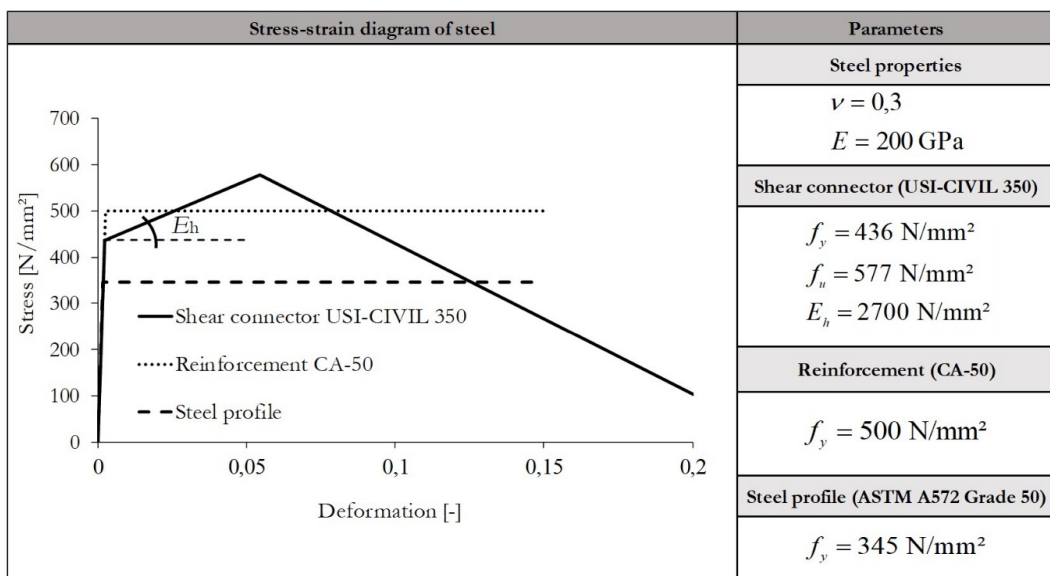


Figure 12. Material model for steel components.

### 4.1.5 Validation

The validation of the numerical model was based on the experimental results of Oliveira [30]. Aspects such as concrete cracking and shear connector deformations were also considered. In Figure 13, the “load-slip” curves obtained in the experiments and numerical models are compared. The maximum load obtained in the experiments and in the numerical models is presented in Table 2.

**Table 2.** Numerical and experimental results.

Specimen	Group	Maximum force of the shear connector		
		Numerical	Test	Ratio
		$F_{m\acute{a}x,num}$ [kN]	$F_{m\acute{a}x,exp}$ [kN]	$F_{m\acute{a}x,num}/F_{m\acute{a}x,exp}$
CR56b PL30iso-As0	D1	296,63	312,78	0,95
CR56b PL30iso-As8	D2	359,00	408,29	0,88
CR56b PL30-As0	D3	306,82	313,09	0,98
CR56b PL45iso-As0	D4	271,90	291,35	0,93
CR56b-As0	D5	331,22	344,37	0,96
			Mean	0,94
			Standard deviation	0,04
			Coefficient of variation	4,07%

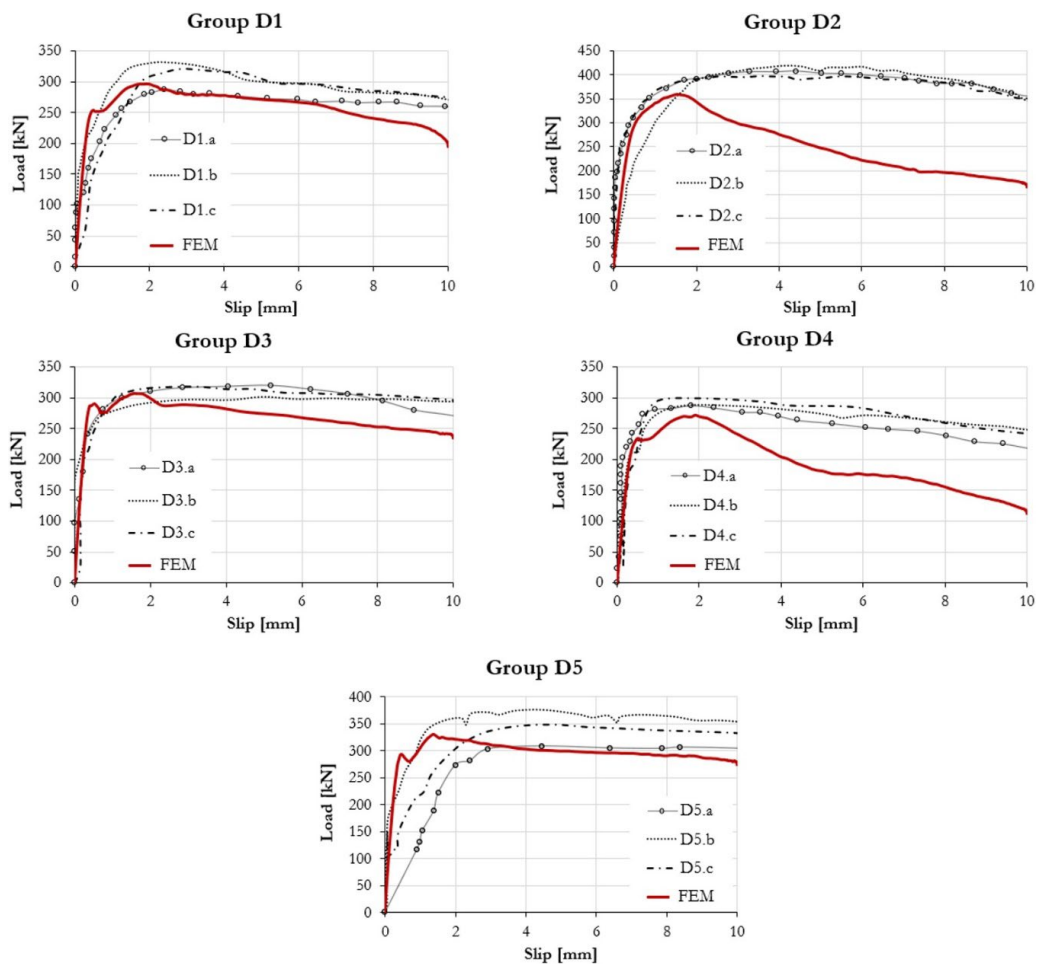


**Figure 13.** Comparison between experimental and numerical “load-slip” curves.

In all cases, the maximum numerical load reached is slightly below the respective experimental value, with a mean ratio of 0,94 and a small coefficient of variation of 4,07% (Table 2). Although the focus of this research is to analyze the behavior of the connection when it reaches its maximum strength, the numerical model was able to simulate the post-peak behavior of groups D1, D3 and D5. Modelling push-out tests in their post-peak stage is a difficult task due to all the contact interactions involved and due to the concrete cracking and plastic deformations present in this stage. The effect of the reinforcement inside the openings of the shear connector was well captured by the numerical model of group D2 in spite of the divergence in the post-peak stage. In general, the numerical model yielded reliable results in comparison to experimental ones, with the highest and lowest shear connector strength in groups D2 and D4, respectively.

In the experiments, cracks were observed on the concrete in the central region of the slab, which would later be expelled, causing the connection to fail (Figure 14a). In the numerical model, this aspect of cracking is simulated very similarly, as shown in Figure 14b.

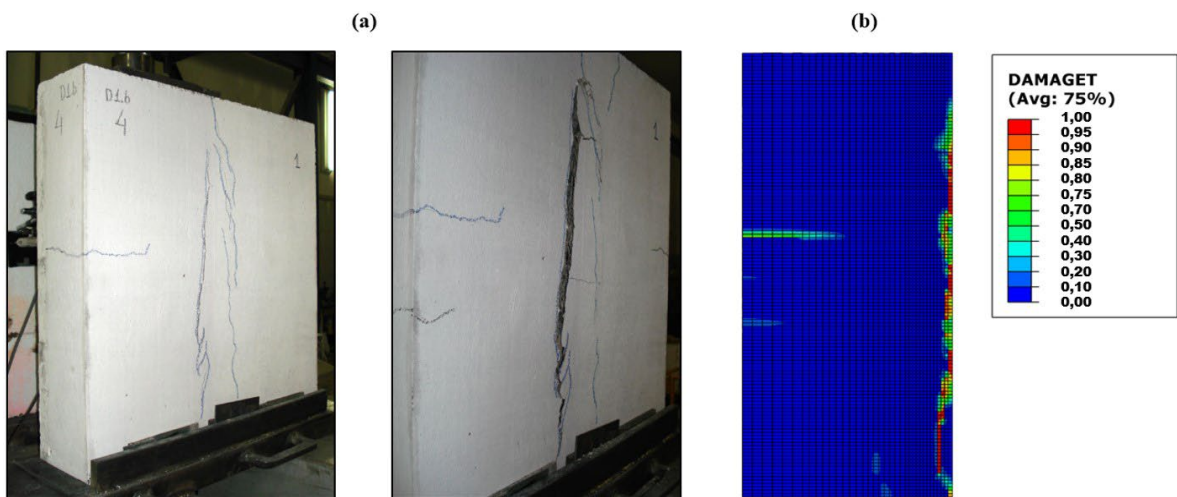


Figure 14. Concrete slab cracking: (a) experiment and (b) numerical model (group D1).

In the specimens with no pre-slab (group D5), a detachment of the concrete located immediately in front of the connector was observed in the internal region of the slab due to the frontal force exerted by the shear connector. In the respective numerical model, this aspect was also observed through tensile damage (Figure 15).

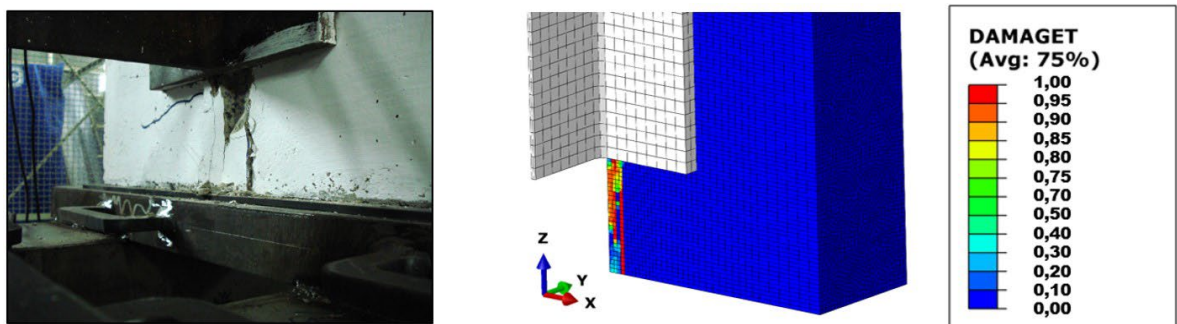


Figure 15. Concrete cracking in front of the shear connector.

According to Oliveira [30], in all experiments, the shear connector did not suffer significant deformations, remaining practically intact after the tests. For comparison purposes, the numerical model of group D3 is illustrated in Figure 16 in which the maximum stress reached by the shear connector (451,87 MPa) is highlighted. This value is slightly higher

than the yield stress ( $f_y = 436$  MPa) of the shear connector and was identified in a small region in the steel dowel, corroborating the observations of Oliveira [30].

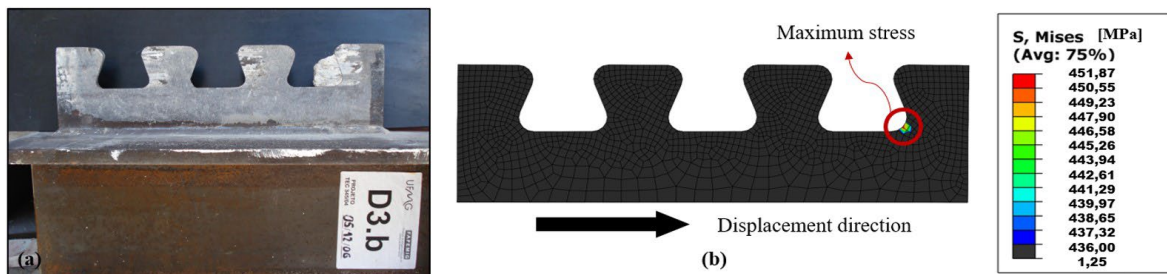


Figure 16. (a) Shear connector after tests; (b) stresses in numerical model (group D3).

In all experiments, the rupture was caused by a specific concrete failure mode since the connector remained practically intact in all tests. According to Kopp et al. [21], there are two possible failure modes of concrete associated with composite dowels: (a) concrete shearing and (b) concrete pry-out. In the latter case, the rupture is due to the confinement of the concrete that occurs inside the openings of the shear connector, as previously explained. The height of the pry-out cone (see Figure 2) depends on  $c_t$  and  $c_u$  and is one of the main factors that directly affects concrete pry-out resistance.

By associating the values of parameters  $c_t$  and  $c_b$  of the tested specimens (Table 1) with the experimental and numerical results (presented in Table 2), one could conclude that concrete pry-out was the failure mode that occurred during the tests. In fact, since the D4 model has the smallest cover, it was expected to have the lowest capacity among all models, with a pry-out failure in the internal region of the slab. In groups D1 and D2, due to the close values of  $c_t$  and  $c_b$ , the failure could occur on both the inner and outer surface of the slab, while in models D3 and D5 concrete pry-out should only occur on the outer surface, since the upper flange of the steel profile prevents the expulsion of the concrete cone from the inner surface. It is important to highlight that, in specimens with EPS plates, the height of the board was not considered to calculate the concrete cover in the bottom ( $c_b$ ) since the EPS plate would not resist the blow-out force.

The emergence of the fracture surface related to concrete pry-out was checked in numerical models by a cutting plane in the slab 30 mm away from the shear connector (Figure 17). The tensile damage present in numerical models is consistent with the concrete pry-out failure mode described: the pry-out cone was observed on internal (model D4), external (model D3), and in both (model D1) surfaces.

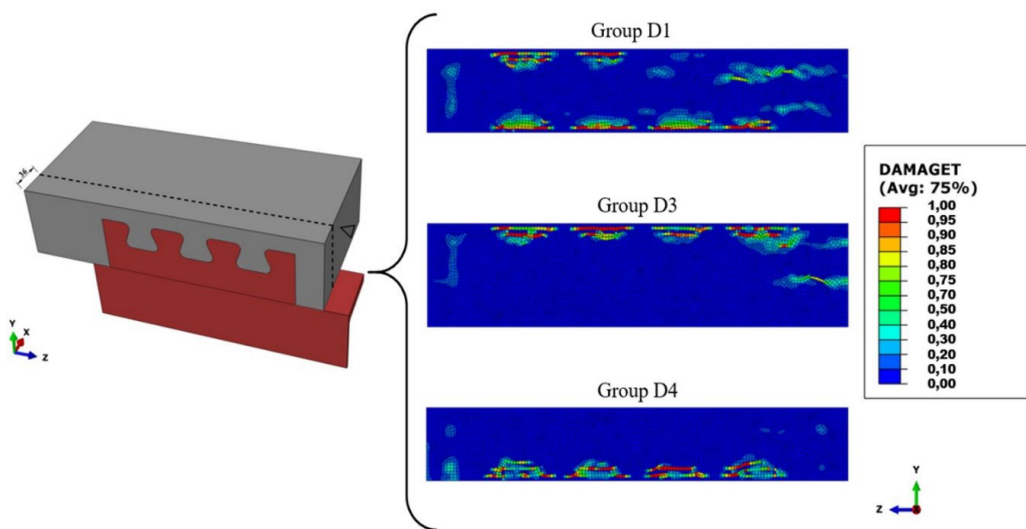


Figure 17. Tensile damage in the concrete slab.

### 4.2 Parametric analysis

A numerical model capable of reproducing concrete pry-out conditions was developed for a single CR50 dowel so that a parametric analysis of its pry-out resistance could be conducted (Figure 18). For this purpose, boundary conditions and reinforcement arrangement were adopted based on the research by Classen and Herbrand [20], where the authors investigated concrete pry-out in puzzle-shaped shear connectors. The reinforcement was adopted in a way that provides the necessary confinement to cause the concrete to pry-out. In addition, a 20 mm thick shear connector with a yield strength of 460 MPa (European high-strength steel S460) was used. These parameters were adopted to avoid steel failure of the shear connector, which would nullify the hypothesis of concrete pry-out. Other properties of the numerical model such as material behaviors, contact interactions, mesh, and analysis method were the same as those of the model used in the validation of the tests.

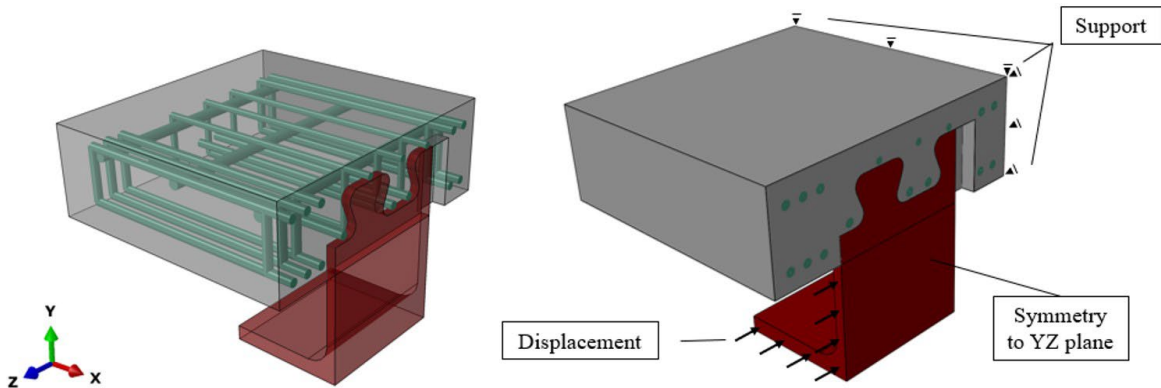


Figure 18. Numerical model developed for the parametric study.

The dimensions of the Crestbond shear connectors are described in terms of dowel spacing ' $e_x$ ' and are shown in Figure 19.

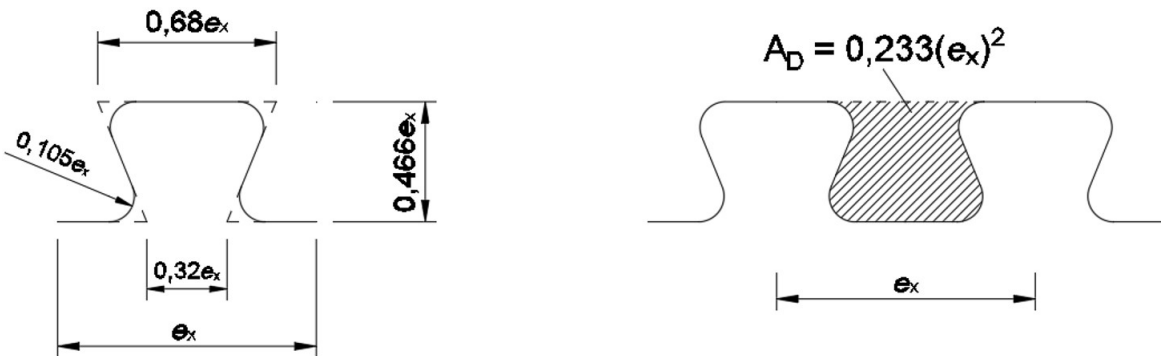


Figure 19. Crestbond dimensions as a function of dowel spacing  $e_x$ .

The main objective of this study was to create a database that would enable the adjustment of Equation 5 for the Crestbond shear connector. The range of all parameters was configured to ensure the occurrence of pry-out in all analyses. A scheme identifying the studied parameters, as well as their range, is presented in Figure 20.

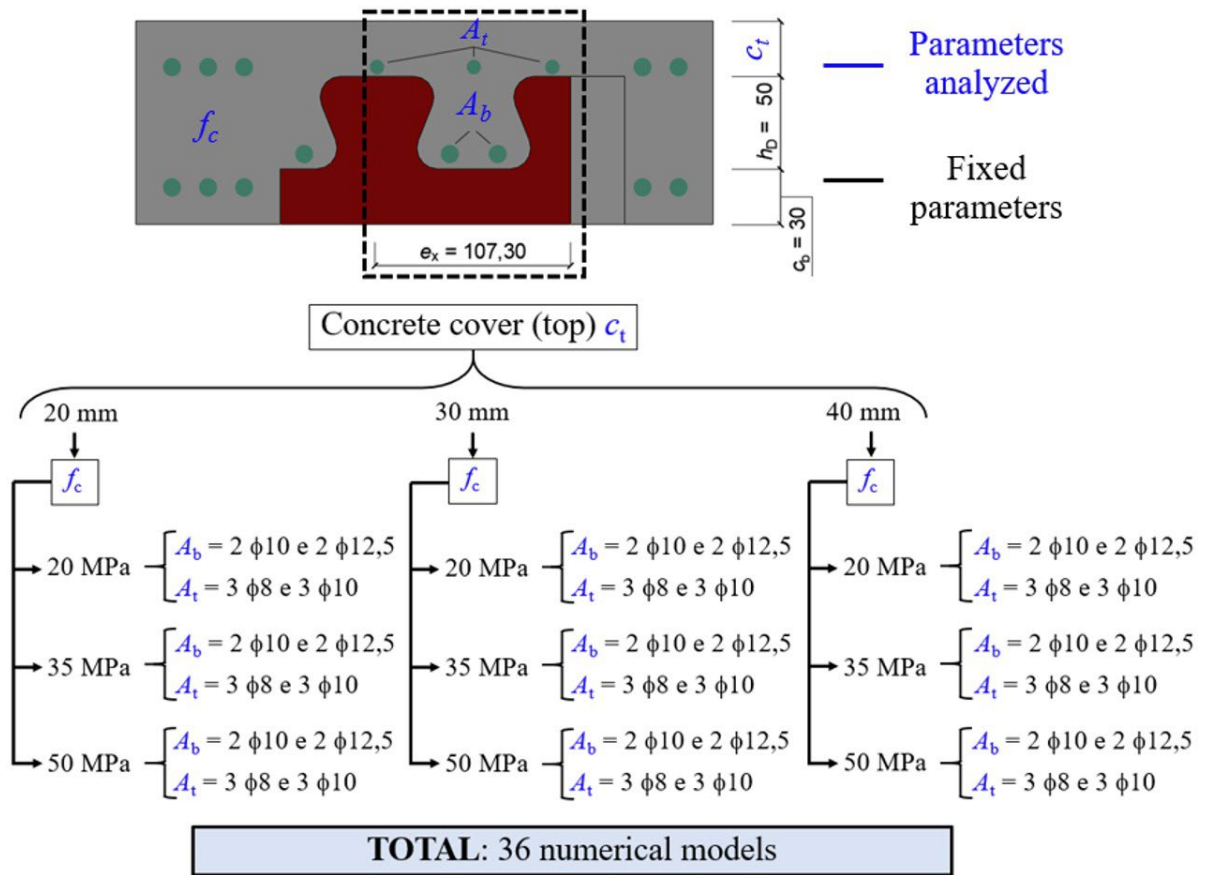


Figure 20. Parametric study (dimensions in mm).

The results of all 36 numerical simulations are shown in Table 3. They were divided according to the height of the concrete slab and the nomenclature of the models following the designation shown in Figure 21.



Figure 21. Example of nomenclature.

**Table 3.** Numerical results of the parametric study.

	Model	Maximum force [kN]	Model	Maximum force [kN]	Model	Maximum force [kN]		
Height of the slab ( $h_c$ ) = 100 mm	fc20-Ab10-At8	125,21	Height of the slab ( $h_c$ ) = 110 mm	fc20-Ab10-At8	132,65	Height of the slab ( $h_c$ ) = 120 mm	fc20-Ab10-At8	133,82
	fc20-Ab10-At10	128,28		fc20-Ab10-At10	135,98		fc20-Ab10-At10	136,45
	fc20-Ab125-At8	130,47		fc20-Ab125-At8	138,32		fc20-Ab125-At8	138,77
	fc20-Ab125-At10	133,13		fc20-Ab125-At10	141,05		fc20-Ab125-At10	140,29
	fc35-Ab10-At8	162,54		fc35-Ab10-At8	171,01		fc35-Ab10-At8	173,78
	fc35-Ab10-At10	167,18		fc35-Ab10-At10	176,47		fc35-Ab10-At10	177,94
	fc35-Ab125-At8	173,28		fc35-Ab125-At8	181,78		fc35-Ab125-At8	183,71
	fc35-Ab125-At10	177,85		fc35-Ab125-At10	185,88		fc35-Ab125-At10	188,42
	fc50-Ab10-At8	192,95		fc50-Ab10-At8	199,87		fc50-Ab10-At8	209,27
	fc50-Ab10-At10	199,14		fc50-Ab10-At10	208,64		fc50-Ab10-At10	213,09
fc50-Ab125-At8	201,69	fc50-Ab125-At8	206,75	fc50-Ab125-At8	216,56			
fc50-Ab125-At10	208,47	fc50-Ab125-At10	215,35	fc50-Ab125-At10	220,77			

The results of all models were analyzed in order to verify the failure by concrete pry-out. Below, evidence is presented identifying this failure mode in the numerical model where its occurrence is the most unlikely, since it is the one with the highest concrete strength (50 MPa) and slab height (120 mm).

In Figure 22, tensile damage in the maximum force increment of the fc50-Ab125-At10 model indicates a cracking aspect similar to the formation of the pry-out cone, with damage appearing near the tips of the shear connector and progressing towards the slab's upper surface.

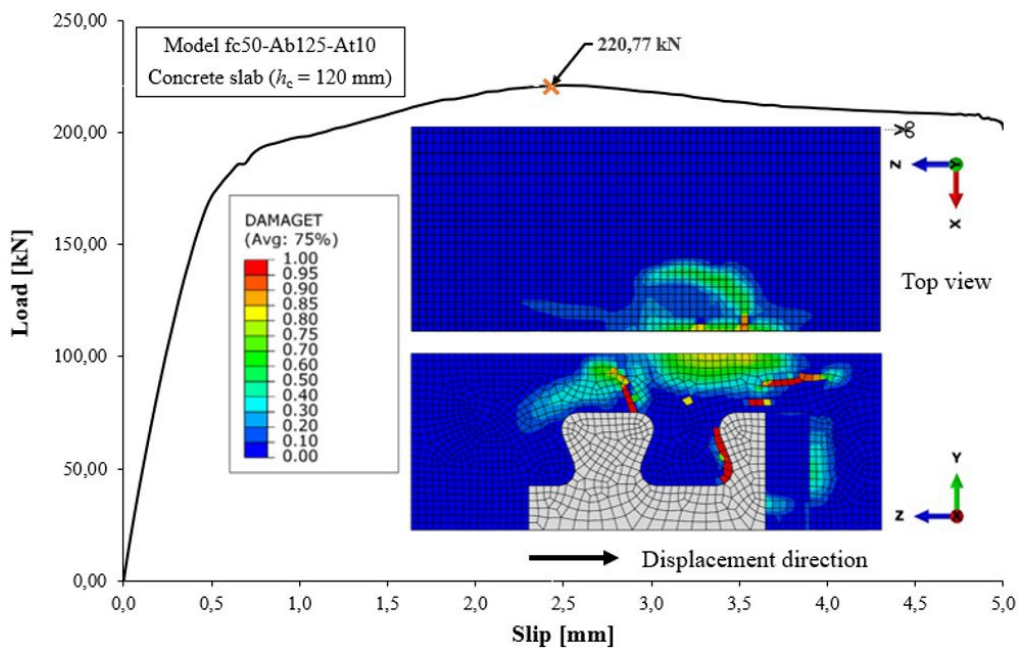


**Figure 22.** Load-slip curve of 'fc50-Ab125-At10' model ( $h_c = 120$  mm).

In Figure 23, there is a good correspondence between the tensile damage of the numerical model and the cracking pattern observed in the experiments conducted by Classen and Herbrand [20] with puzzle shear connectors. Another aspect that should be highlighted is that a vertical displacement of a concrete portion was observed in the numerical simulations, caused by the outward pry-out force (Figure 24).

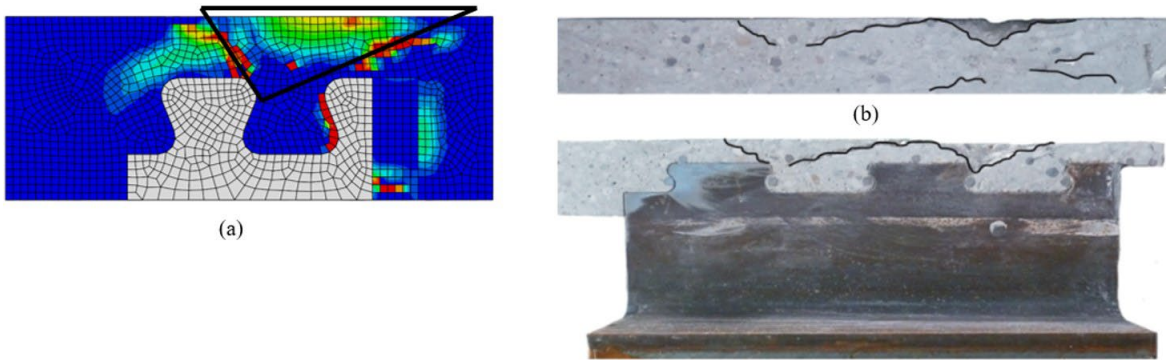


**Figure 23.** (a) Tensile damage in numerical model; (b) concrete cracking in experiments with puzzle shear connector – Classen and Herbrand [20].

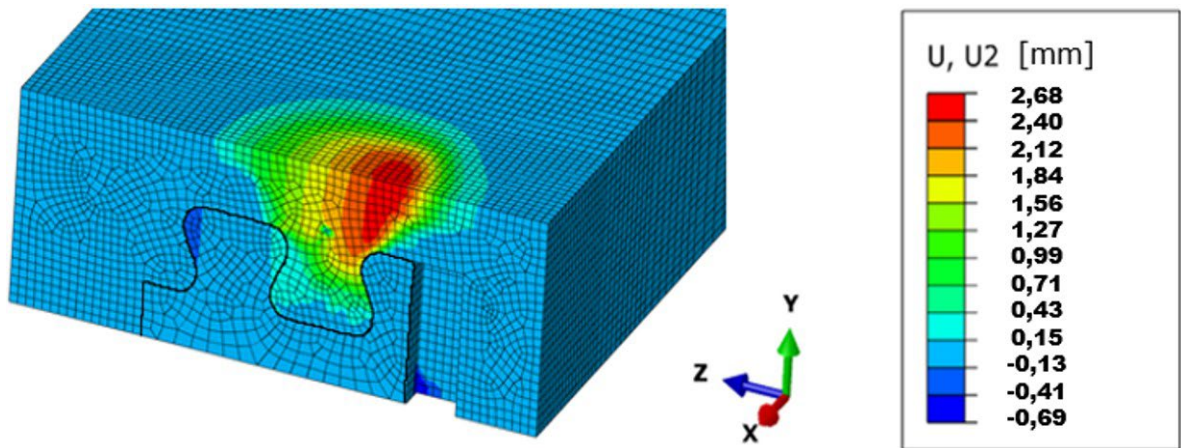


**Figure 24.** Vertical displacement of concrete due to pry-out.

Finally, tensile damage was verified in the same section of the slab (30 mm from the shear connector) as presented in Figure 17. The similarity between the cracking aspect of the model based on Verissimo's experiments and the single dowel model is evident (Figure 25).

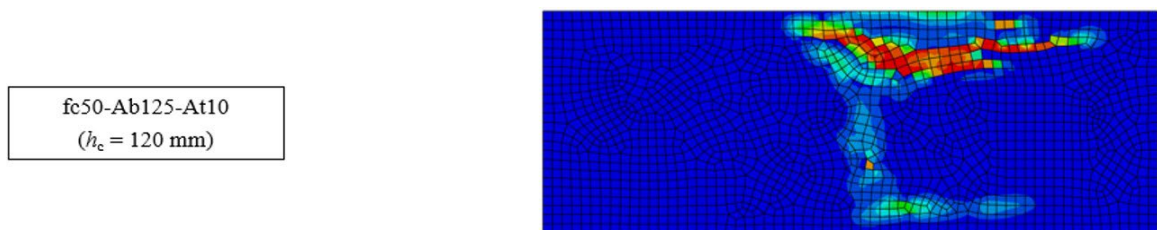


**Figure 25.** Tensile damage comparison between group D3 and fc50-Ab125-At10 ( $h_c = 120$  mm).

Considering that no steel damage was observed in the shear connector of the single dowel model, and due to the similarity of the cracking aspect of all three push-out models (physical, numerical, and single dowel), one can conclude that concrete pry-out is the failure mode occurring in all of these cases. Therefore, the results of the single dowel model's parametric analysis can be used to calibrate the analytical model.

### 5 MECHANICAL MODEL AND COMPARISON WITH EXPERIMENTAL RESULT

The mechanical model presented in Equation 5 was used to estimate Crestbond’s resistance to concrete pry-out considering only one row of shear connectors ( $\chi_y = 1,0$ ). The height of the concrete cone was calculated according to Equation 4, valid for PZ and MCL geometries. In this work, the ‘k’ coefficient was determined using the results of the parametric study through a regression analysis, and the value obtained was 37 (Equation 7), which results in a mean  $P_{theo}/P_{FEM}$  value equal to 0,91 and a coefficient of variation of 24,24%.

$$P_{po,CR} = 37 \frac{1}{\eta} (1 + \rho_{D,i}) \chi_x \sqrt{f_{ck}} h_{po}^{1,5} \tag{7}$$

Finally, experimental results were compared with those obtained through Equation 7 (Figure 26), in which a mean ratio  $P_{theo}/P_{exp}$  of 0,99 and a coefficient of variation of 10% were obtained. The coherence of the mechanical model is especially evident when its results are compared with those of group D4. Due to the small concrete cover ( $c_b = 15$  mm), there is a high probability of concrete pry-out in specimens of this group, and this is evident in the extremely close values between  $P_{theo}$  and  $P_{exp}$ . This is consistent with Figure 27b, where a vertical displacement (in the direction of the smallest concrete cover -  $c_b$ ) was observed.

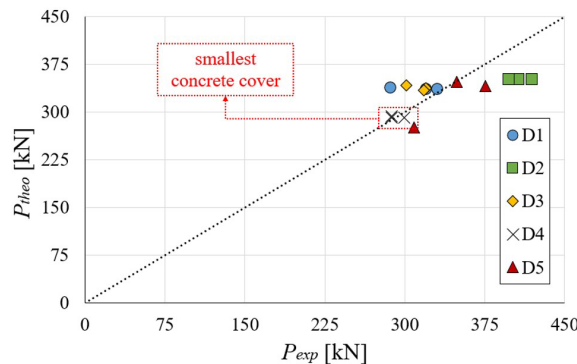


**Figure 26.** Comparison between experimental and analytical results.

The influence of the reinforcement is clearly visible when comparing the results of groups D1 and D2, which have the same concrete cover on both sides. Although the mechanical model takes the effect of the reinforcement into consideration, it is clear that its contribution to the connection’s resistance is greater in the experimental values. In general, the errors between theoretical and experimental results did not exceed 15%, which demonstrates the consistency of the mechanical model.

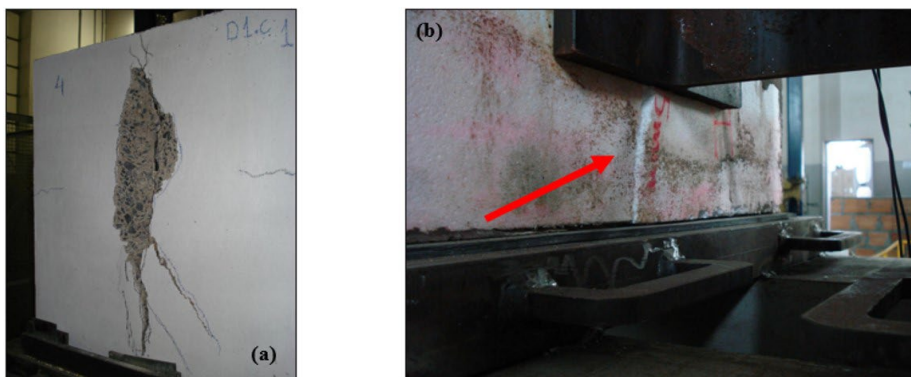


**Figure 27.** Typical cracking of concrete pry-out observed in tests: (a) D1 and (b) D4.

## 7 CONCLUSIONS

In this paper, a mechanical model was proposed to estimate the concrete pry-out resistance of Crestbond shear connectors. The model was based on already established expressions currently in use for shear connectors with puzzle and clothoidal geometries. The proposed expression was adjusted through a parametric study involving numerical simulations capable of representing the concrete pry-out failure mode. Explicit dynamic analysis was conducted and it proved to be effective in validating the numerical model, presenting a mean ratio between numerical and experimental results equal to 0,94 and a small coefficient of variation of 4,07%. The validation of the models for concrete pry-out was performed through an analysis between the concrete tensile damage observed in the numerical model and the cracking aspect in experiments. The proposed equation corresponded well to the experimental results, with a mean ratio  $P_{theo}/P_{exp}$  equal to 0,99 and a coefficient of variation of 10%. The values found in this study suggest that the concrete pry-out expressions in German Technical Approval Z-26.4-56 [22] can also be applied to Crestbond shear connectors. An analysis of the structural behavior of Crestbond shear connectors in full-size beams subjected to monotonic loads is suggested as a subject for future research for the purpose of evaluating the consistency and applicability of the proposed expressions.

## 8 ACKNOWLEDGEMENTS

The authors wish to acknowledge the *Coordenação de Aperfeiçoamento de Pessoal de Nível Superior – CAPES* (Coordination for the Improvement of Persons in Higher Education) – Finance Code 001, *Universidade Federal de Viçosa*, and *Conselho Nacional de Desenvolvimento Científico e Tecnológico – CNPq* (National Council of Scientific and Technological Development) for their support in the realization and dissemination of this study.

## 9 REFERENCES

- [1] W. Lorenc, "The model for a general composite section resulting from the introduction of composite dowels," *Steel Constr.*, vol. 10, no. 2, pp. 154–167, May 2017, <http://dx.doi.org/10.1002/stco.201710019>.
- [2] M. Feldmann, M. Kopp, and D. Pak, "Composite dowels as shear connectors for composite beams – background to the German technical approval," *Steel Constr.*, vol. 9, no. 2, pp. 80–88, May 2016, <http://dx.doi.org/10.1002/stco.201610020>.
- [3] G. Seidl et al., "Composite Dowels in Bridges - Efficient solution," *Adv. Mat. Res.*, vol. 814, pp. 193–206, Sep 2013, <http://dx.doi.org/10.4028/www.scientific.net/AMR.814.193>.
- [4] O. Hechler et al. "Continuous Shear Connectors in Bridge Construction," in *Int. Conf. Compos. Constr. Steel and Concr.*, Devil's Thumb Ranch, Tabernash, Colorado, USA, July 20-24, 2008.
- [5] G. Seidl et al. *Prefabricated Enduring Composite Beams Based on Innovative Shear Transmission: Design Guide*, Brussels, 2013.
- [6] W. Lorenc, M. Kożuch, and S. Rowiński, "The behaviour of puzzle-shaped composite dowels — Part I: Experimental study," *J. Construct. Steel Res.*, vol. 101, pp. 482–499, Oct 2014, <http://dx.doi.org/10.1016/j.jcsr.2014.05.013>.
- [7] W. Lorenc, M. Kożuch, and S. Rowiński, "The behaviour of puzzle-shaped composite dowels - Part II: Theoretical investigations," *J. Construct. Steel Res.*, vol. 101, pp. 500–518, Oct 2014, <http://dx.doi.org/10.1016/j.jcsr.2014.05.012>.
- [8] M. Classen and J. Gallwoszus, "Concrete fatigue in composite dowels," *Struct. Concr.*, vol. 17, no. 1, pp. 63–73, Apr 2016., <http://dx.doi.org/10.1002/suco.201400120>.
- [9] G. S. Veríssimo, "Desenvolvimento de um conector de cisalhamento em chapa dentada para estruturas mistas de aço e concreto e estudo do seu comportamento," Ph.D. dissertation, Esc. de Engenharia, Univ. Fed. de Minas Gerais, Belo Horizonte, Minas Gerais, 2007.
- [10] O. P. Aguiar et al., "Estudo de conectores Crestbond em pilares mistos preenchidos com concreto," *Rev. Estr. Aco.*, vol. 4, no. 3, pp. 181–199, Dec 2015.
- [11] O. P. Aguiar, R. B. Caldas, F. C. Rodrigues, R. H. Fakury, and G. S. Veríssimo, "Crestbond shear connectors for load transfer in concrete filled tube columns," *Ibrac. Struct. Mater. J.*, vol. 11, no. 5, pp. 960–965, Oct 2018, <http://dx.doi.org/10.1590/s1983-41952018000500004>.
- [12] A. R. Alves, B. V. Isabel, B. V. Washintgon, and S. V. Gustavo, "Prospective study on the behavior of composite beams with an indented shear connector," *J. Construct. Steel Res.*, vol. 148, pp. 508–524, Sep 2018, <http://dx.doi.org/10.1016/j.jcsr.2018.06.015>.
- [13] H. S. Cardoso, R. B. Caldas, R. H. Fakury, and G. S. Veríssimo, "Estudo do Comportamento de Conectores Crestbond por meio de Simulação Numérica," *Rev. Estr. Aco.*, vol. 7, no. 2, pp. 140–159, Aug 2018, <http://dx.doi.org/10.17648/aco-2238-9377-7-2-4>.
- [14] H. S. Cardoso, R. B. Caldas, R. H. Fakury, G. S. Veríssimo, and R. L. J. Almeida, "Modelo de cálculo para o cisalhamento do concreto nos conectores Crestbond," *Rev. Estr. Aco.*, vol. 7, no. 3, pp. 280–299, Dec 2018, <http://dx.doi.org/10.17648/aco-2238-9377-7-3-3>.

- [15] H. S. Cardoso, O. P. Aguiar, R. B. Caldas, and R. H. Fakury, "Composite dowels as load introduction devices in concrete-filled steel tubular columns," *Eng. Struct.*, vol. 219, pp. 110805, Sep 2020, <http://dx.doi.org/10.1016/j.engstruct.2020.110805>.
- [16] Almeida et al., "Capacidade resistente do conector Crestbond à falha do aço desencadeada por um mecanismo combinado de cisalhamento e flexão," *Rev. Estr. Aco*, vol. 9, no. 1, pp. 61–80, Apr 2020, <http://dx.doi.org/10.17648/aco-2238-9377-9-1-3>.
- [17] W. Lorenc, "Concrete failure of composite dowels under cyclic loading during full-scale tests of beams for the "Wiarna Rzeki" bridge," *Eng. Struct.*, vol. 209, pp. 110199, Apr 2020, <http://dx.doi.org/10.1016/j.engstruct.2020.110199>.
- [18] M. Kozüch and W. Lorenc, "Stress concentration factors of shear connection by composite dowels with MCL shape," *Arch. Civ. Mech. Eng.*, vol. 19, no. 1, pp. 32–46, Mar 2019, <http://dx.doi.org/10.1016/j.acme.2018.08.006>.
- [19] M. Kozüch and W. Lorenc, "The behaviour of clothoid-shaped composite dowels: Experimental and numerical investigations," *J. Construct. Steel Res.*, vol. 167, pp. 105962, Apr 2020, <http://dx.doi.org/10.1016/j.jcsr.2020.105962>.
- [20] M. Classen and M. Herbrand, "Shear behavior of composite dowels in transversely cracked concrete," *Struct. Concr.*, vol. 16, no. 1, pp. 195–206, Dec 2014, <http://dx.doi.org/10.1002/suco.201400100>.
- [21] M. Kopp et al., "Composite dowels as shear connectors for composite beams – background to the design concept for static loading," *J. Construct. Steel Res.*, vol. 147, pp. 488–503, Aug 2018, <http://dx.doi.org/10.1016/j.jcsr.2018.04.013>.
- [22] Allgemeine bauaufsichtliche Zulassung der Verbunddübelsteife, no. Z-26.4-56, Berlin: Deutsches Institut für Bautechnik, 2018.
- [23] C. M. Dutra, "Estudo do comportamento estrutural do conector Crestbond considerando variações geométricas e mecânicas," M.S. thesis, Univ. Fed. de Viçosa, Viçosa, Minas Gerais, 2014.
- [24] M. Classen and J. Hegger, "Assessing the pry-out resistance of open rib shear connectors in cracked concrete – Engineering model with aggregate interlock," *Eng. Struct.*, vol. 148, pp. 254–262, Oct 2017, <http://dx.doi.org/10.1016/j.engstruct.2017.06.050>.
- [25] C. Zapfe, "Trag- und Verformungsverhalten von Verbundträgern mit Betondübeln zur Übertragung der Längsschubkräfte," Ph.D. dissertation, Institut für Konstruktiven Ingenieurbau, Universität der Bundeswehr, München, 2001.
- [26] G. Seidl, "Behavior and load bearing capacity of composite dowels in steel-concrete composite girders," Ph.D. dissertation, Wrocław Univ. of Tech., Wrocław, 2009.
- [27] S. Heinemeyer "Zum Trag- und Verformungsverhalten von Verbundträgern aus ultrahochfestem Beton mit Verbundleisten," Ph.D. dissertation, Rheinisch-Westfälischen Technischen Hochschule, Aachen, 2011.
- [28] The European Union. *Basis of Structural Design*, EN 1990:2002, 2002.
- [29] The European Union. *Design of Composite Steel and Concrete Structures. Part 1-1: General Rules and Rules for Buildings*, EN1994-1-1, Dec. 2004.
- [30] A. F. N. Oliveira "Análise do comportamento de um conector de cisalhamento em chapa dentada para sistemas de pisos mistos com pré-laje de concreto," M.S. thesis, Esc. de Engenharia, Univ. Fed. de Minas Gerais, Belo Horizonte, 2007.
- [31] S. Zheng, Y. Liu, T. Yoda, and W. Lin, "Parametric study on shear capacity of circular-hole and long-hole perfbond shear connector," *J. Construct. Steel Res.*, vol. 117, pp. 64–80, Feb 2016, <http://dx.doi.org/10.1016/j.jcsr.2015.09.012>.
- [32] M. Pavlovic, Z. Marković, M. Veljković, and D. Buđevac, "Bolted shear connectors vs. headed studs behaviour in push-out tests," *J. Construct. Steel Res.*, vol. 88, pp. 134–149, Sep 2013, <http://dx.doi.org/10.1016/j.jcsr.2013.05.003>.
- [33] J. Fink et al., "Weitere neue Dübelformen für Verbundbau und numerische Simulation von PushOut-Versuchen mit ABAQUS," Vienna, 2007. Report for TU.
- [34] H. P. Silva, "Simulação numérica do comportamento de conectores de cisalhamento tipo Crestbond," M.S. thesis, Univ. Fed. de Viçosa, Viçosa, Minas Gerais, 2013.
- [35] SIMULIA, *ABAQUS analysis user's manual*. Providence, USA, 2012.
- [36] M. Classen, "Limitations on the use of partial shear connection in composite beams with steel T-sections and uniformly spaced rib shear connectors," *J. Construct. Steel Res.*, vol. 142, pp. 99–112, Mar 2018, <http://dx.doi.org/10.1016/j.jcsr.2017.11.023>.
- [37] The European Union. *Design of Concrete Structures. Part 1-1: General Rules and Rules for Buildings*, EN1992-1-1, 2010.
- [38] D. A. Hordijk, "Local approach to fatigue of concrete," Ph.D. dissertation, Delft Univ. of Tech., Delft, 1991.
- [39] Fédération Internationale du Béton, *Model Code 2010: Final Draft*, Lausanne, Switzerland: FIB, 2011.
- [40] M. P. Byfield and M. Dhanalakshmi, "Analysis of strain hardening in steel beams using mill tests," *Adv. Steel Struct*, vol. 1, pp. 139–146, 2002, <http://dx.doi.org/10.1016/B978-008044017-0/50015-9>.

---

**Author contributions:** RLJA: conceptualization, writing, data curation and formal analysis; GSV: supervision, methodology and review; JCLR and RBC: methodology and review; HSC and JLRP: review; RHF: funding acquisition and review.

**Editors:** Yury Andrés Villagrán Zaccardi, Guilherme Aris Parsekian.